

Unveiling Hidden Physics in the 215-Kelvin Superconducting Calcium Hydride: Temperature, Quantum and Defect Effects

Hui Wang^{1,†}, Xiaoqiu Ye², Xitian Zhang¹, Jian Lv^{3,‡}, and Yansun Yao⁴

¹Key Laboratory for Photonic and Electronic Bandgap Materials (Ministry of Education), School of Physics and Electronic Engineering,
Harbin Normal University, Harbin 150025, China

²Science and Technology on Surface Physics and Chemistry Laboratory, Jiangyou, 621908, China

³International Center for Computational Method & Software, College of Physics, Jilin University, Changchun 130012, China

⁴Department of Physics and Engineering Physics, University of Saskatchewan, Saskatoon, Saskatchewan S7N 5E2, Canada

[†]wh@fysik.cn; [‡]lvjian@calypso.cn

Temperature and quantum effects induce the structural complexity of condensed hydrogen, and therefore they are expected to impact nontrivially the structures of clathrate hydrides. Exemplified by clathrate calcium hydride, we show through *ab initio* (path-integral) molecular dynamics simulations that these effects are indeed pivotal at 100-200 GPa. The quantum equation of states derived at 300 K suggests that the synthesized samples in previous experiments were berthollide-like $\text{CaH}_{6-\delta}$, with the stoichiometric defect δ increasing smoothly during decompression. The change of composition provides an explanation for the experimental observation of positive pressure dependence of superconducting T_c below 165 GPa. Furthermore, we find significant proton diffusion in $\text{CaH}_{6-\delta}$ at 150-300 K, with the diffusion coefficient reaching $10^{-7} \text{ cm}^2/\text{s}$. This suggests a coexistence of superconductivity and proton diffusion in clathrate hydrides. Our findings underline the importance of temperature, quantum and defect effects to the understandings of the structure and pertinent physics in high- T_c superconducting clathrate hydrides.

In 1968, Ashcroft theorized in his seminal paper[1] that if the hydrogen molecule is dissociated and a purely atomic alkali-metal-like solid is formed[2], this solid could exhibit room temperature superconductivity. The solid atomic hydrogen (SAH) is still beyond the experimental reach[3-5], but a class of close alternatives has been discovered recently at megabars, *i.e.* clathrate hydrides[6]. In clathrate hydrides, metal atoms form a host lattice that accommodates hydrogen atoms in interstitial sites. The nearest H-H distances approach the theoretical value predicted for SAH[7], through which the hydrogen atoms are connected into sodalite-like cages[8]. At present, near room temperature superconductivity has been discovered in clathrate hydrides synthesized in La-H[9,10], Y-H[11,12] and La-Y-H[13] systems. This new family of materials is being intensively explored for room-temperature superconductivity, both in theory and experiment[14-16].

As hydrogen is the lightest element, the thermal and quantum motions of its nucleus strongly affect the structural properties of condensed hydrogen at near room temperature, as revealed by the intriguing phenomena of temperature-induced phase III-IV transition [17,18] and lattice fluxionality of phase IV[19,20]. The structural similarity to SAH thus points to the importance of quantum and temperature effects in clathrate hydrides. Recently, it is theorized that the inclusion of quantum atomic fluctuation is required for correct evaluation of the pressure boundary and superconducting critical temperature T_c of LaH₁₀[21]. This study unveils the quantum structural nature of clathrate hydrides. Moreover, it is also found in LaH_{9.6} that vacancy defects facilitate the quantum motion of proton, and this can result in an appreciable structural fluxion at low temperature[22]. These findings suggest that the quantum, temperature and defect effects would be significant in clathrate hydrides.

Due to the difficulties in locating hydrogen in x-ray diffraction (XRD) measurements, clathrate hydrides usually have undetermined hydrogen positions [16]. In experiments, the hydrogen positions are set in the interstitial sites of the host lattice, together with the number of hydrogen atoms counted from the volume difference between hydrides and pure metal. In this way, experimental studies generally report imperfect stoichiometries, *e.g.*, LaH_{9.6}[10] and CeH_{9.8}[23]. However, in experiment-simulation combined studies, the position and number of hydrogen atoms are generally inferred based on comparison between the experimental equation of states (EoS) measured at room temperature and the theoretical EoSs calculated for ideal crystals at zero temperature[16]. The caveat is that the comparison introduces an approximation: The contributions from thermal and quantum motions of nuclei and stoichiometric defect to experimental EoSs are neglectable. This comparison has been commonly used and usually it points to perfect stoichiometries, *e.g.* ThH₁₀[24] and CaH₆[25], but rarely critically examined.

The 215-kelvin superconducting calcium hydride has an experimentally determined body-centered cubic (*bcc*) lattice for calcium atoms[25,26]. In this lattice, a nearly full occupation of tetragonal interstitial sites (Wyckoff position: $12d$) by hydrogen atom yields a CaH_{6- δ} hydride with a small δ (a full occupation would result in CaH₆). In this study, we select CaH_{6- δ} as an example to study the physics of temperature, quantum and defect effects with two considerations: I) noninvolvement of *f* electrons helps to reduce the uncertainty of density functional theory (DFT), as known from counterexamples in lanthanide and actinide hydrides, *e.g.* EuH₆[27]; II) symmetry-equivalent hydrogen sites eliminate the effects of different site symmetries, as opposed to higher hydrides possessing inequivalent hydrogen sites, *e.g.* LaH_{9.6}[10].

To illustrate temperature, quantum and defect effects, we simulate the 300-kelvin EoSs of the CaH_{6- δ} (with δ of 0 and 0.5) in a scenario of quantum structure by path-integral molecular dynamics (PIMD)[28,29], and derive the relative volume shift (δV) with respect to the zero-kelvin EoSs of static structure. From the results presented in Fig. 1, a lower hydrogen content generally corresponds to a smaller δV , *e.g.*, an increment of δ from 0 to 0.5 would result in a reduction of δV from 3.3 % to 2.5 % at 100 GPa. Moreover, δV depends negatively on pressure as expected from the Birch's equation of state for solids[30]. To get the individual contribution of thermal or quantum nuclear motions to δV (denoted as δV_T or δV_Q), we further simulate the 300-kelvin EoSs using a classical structure by molecular dynamics (MD). Subsequently, δV_T is derived in the same way as that of δV , and δV_Q is obtained by subtracting δV_T from δV . It is found that the pressure dependence of δV_Q is much weaker than that of δV_T , due to the quantum nuclear delocalization originated from the extension of the nuclear wavefunction being less sensitive to external thermodynamic environments. As a results, thermal and quantum effects dominate the volume shift at low and high pressures, respectively.

It is not uncommon for a metal-hydrogen system to form a berthollide phase[31], where the lattice symmetry of host metal is stable over a wide range of hydrogen content, *e.g.*, CeH_{2+x} in a face-centered cubic (*fcc*) phase[32]. Unexpectedly, a pressure dependent x has been found in clathrate cerium deuteride: the x in *fcc*- CeD_{9+x} phase reduces smoothly when the pressure is reduced from 140 to 110 GPa[33]. This finding suggests a possibility of changing the concentration of vacancy defects in a synthesized clathrate hydride at different pressures. Obviously, whether such a change is accounted would impact the analysis of the experimental EoSs, as well as other physical properties, *e.g.* electronic structure and proton dynamics.

Since PIMD simulation is capable of revealing the berthollide-like behavior of *fcc*- CeD_{9+x} discovered experimentally (Fig. S1, [34]), it is desirable to reanalyze the experimental EoSs of the clathrate calcium hydride with respect to the PIMD results. As shown in Fig. 2a, a direct comparison between experimental and theoretical EoSs suggests a possible pressure-induced variation of hydrogen content in some experimental samples, indicating the formation of berthollide-like $\text{CaH}_{6-\delta}$ phase, as opposite to stoichiometric CaH_6 reported previously[25]. Specifically, vacancy remains constant in sample 1 in the whole pressure range, with δ averaging about 0.28. In sample 2 and 3, the vacancy concentrations are clearly lower than that in sample 1 at high pressures (>160 or 150 GPa respectively), but they increase to δ of about 0.4 at lower pressures (Fig. S2).

The high hydrogen content accounts for the high-temperature superconductivity of clathrate hydrides, and a reduction is expected (empirically) to suppress superconductivity. Indeed, the pressure range (*i.e.* 135-165 GPa) where the T_c decreases with the pressure in the experimental samples coincides the ‘H losing region’ revealed in Fig. 2a. To get a deep insight, we analyze the dependence of the electronic density of states at the Fermi level $N(\epsilon_F)$ on δ in $\text{CaH}_{6-\delta}$, mimicking a linear dependence of δ on pressure between 135-165 GPa (Fig. S2). The quantum $N(\epsilon_F)$ is calculated by a statistic average over the $N(\epsilon_F)$ of various centroid configurations sampled from PIMD simulations at 300 K, which turn out to depend negatively on δ (or positively on pressure), as shown in Fig. 2b. This trend is robust against the lattice contraction induced by lowering the temperature to T_c . Although correlated to δ variation, the trend cannot be understood from a change of electron numbers in static structure alone, *e.g.*, the rigid band model[39] of the electronic structure of CaH_6 , which predicts an opposite trend (Fig. 2b). Instead, the trend seems to be a consequence of diverse distortions of the dynamical structure (Fig. S4), within which the XRD constraints are still satisfied (Fig. S5). According to the Bardeen-Cooper-Schrieffer (BCS) theory[40], $N(\epsilon_F)$ and T_c generally exhibit the same pressure trend in high- T_c hydrides, *e.g.* the dome-shaped pressure trend in $\text{LaH}_{9,6}$ [22]. The trend of the statistic $N(\epsilon_F)$ in $\text{CaH}_{6-\delta}$ thus supports preliminarily the empirical expectation. The positive pressure dependence of T_c found in experiments below 165 GPa contradicts to early prediction[8], and was attributed empirically to structural distortions of CaH_6 [25]. Here, the variation of hydrogen content and resulted structural changes of $\text{CaH}_{6-\delta}$ provide an alternative and complementary explanation.

The nearest distance between interstitial d sites at pressures of 123-190 GPa was measured on average to be 1.24 Å, which corresponds to an energy barrier of 155 meV for vacancy migration in CaH_6 crystal (Fig. S6). Notably, the zero-point energy (ZPE) in CaH_6 (about 200 meV) already exceeds the barrier, which would result in nontrivial proton dynamics in $\text{CaH}_{6-\delta}$. Taking $\text{CaH}_{5.74}$ at 160 GPa as an example, we explore the proton dynamics by ring polymer molecular dynamics (RPMD) with a quantum-mechanical treatment of nuclei. As shown in Fig. 3a, the mean square displacement (MSD), $\langle u^2 \rangle$, reveals significant proton diffusion about the interstitial sites at 150-300 K. The diffusion coefficient D reaches to about 8.7×10^{-8} - 4.3×10^{-7} cm²/s and increases positively with the temperature. Switching from quantum to classical treatment of nuclei (*i.e.* RPMD to MD) would reduce the D value to 2.0×10^{-8} - 2.7×10^{-7} cm²/s. This suggests that thermal effects impact the diffusion more significantly than nuclear quantum effects at the studied temperatures, and more so at higher temperatures. Moreover, the crucial role of vacancies played in diffusion is demonstrated through a comparison to the dynamics of CaH_6 . The latter exhibits no diffusion at all at 300 K. Experimentally, superconducting transition was observed in the pressure range of 135-200 GPa at temperatures of about 135-215 K in 12 different samples[25]. Since the samples have a strong possibility to adopt a composition closing to $\text{CaH}_{5.74}$ (Fig. 2a), the superconductivity is very likely to coexist with proton diffusion. The intriguing quantum phenomenon was proposed initially in a model system (*i.e.* $\text{Li}_2\text{MgH}_{16}$ [41]) and later used to understand $\text{LaH}_{9,6}$ hydride discovered recently[10]. Both $\text{Li}_2\text{MgH}_{16}$ and $\text{LaH}_{9,6}$ are ‘*fcc*’ hydrides. Here, the ‘*bcc*’ $\text{CaH}_{6-\delta}$ hydride provides another outstanding case for experimental investigation on this phenomenon.

Diffusion causes the $\text{CaH}_{5.74}$ to not be a single geometry around which the atoms vibrate, but instead one where the protons dynamically explore different vacancies. This structure is analogous to the quantum fluxional structure (QFS) of $\text{LaH}_{9.63}$ (refer to the nuclear density distributions in Fig. S7)[22]. The nuclear wavefunction of motion among the interstices produces on average a tetrahedrally coordinated hydrogen framework in both $\text{CaH}_{5.74}$ and $\text{LaH}_{9.63}$. However, the differences in hydrogen content and host lattice geometry (*i.e.* *bcc* for Ca and *fcc* for La) lead to essential distinctions between the two frameworks, as revealed in the average radial distribution functions (RDF, $g(r)$; Fig. 3b). For example, a notably delayed but sharper peak for the first coordination shell reveals a less dense but more ordered hydrogen framework in $\text{CaH}_{5.74}$ compared to $\text{LaH}_{9.63}$. It is therefore appropriate to view $\text{CaH}_{5.74}$ as a new prototype of fluxional structure for clathrate hydrides. In addition to diffusion, the confinement from Ca lattice is expected to induce strong vibrations of hydrogen in $\text{CaH}_{5.74}$. To capture this feature, we obtain the vibrational density of states (VDOS, $f(\omega)$) from the Fourier transform of the velocity autocorrelation functions in $\text{CaH}_{5.74}$ at 160 GPa. As shown in Fig. 3c, the partial $f(\omega)$ of hydrogen in $\text{CaH}_{5.74}$ primarily falls in a frequency range of 70-250 meV, which essentially coincides with the vibrational range of hydrogen in the 250-kelvin superconducting $\text{LaH}_{10.8}$ at comparable pressures (*e.g.* 163 GPa)[21,22]. This lays a good foundation for the occurrence of strong electron-phonon coupling and high- T_c superconductivity.

A decade after its theorization, high- T_c superconducting clathrate calcium hydride made its way to the real world last year. Taking advantage of the structural simplicity of this superconducting phase, we conducted a case study for the temperature, quantum and defect effects in clathrate hydrides. The inclusion of these effects leads to several intriguing findings, most notably the decompression-induced reduction of the hydrogen content. This study provides an explanation for the unusual positive pressure dependence of T_c observed in experiments, and the fluxional structure at low temperature. These findings suggest that proton diffusion and superconductivity can co-exist in the structure. Along with great experimental achievement, the inadequacy of modeling clathrate hydrides using static lattice is gradually being recognized in recent years. The present study, together with several recent theoretical studies beyond the static model[21,22,41,42], call for the use of a kind of ‘big model’ to include these effects in the investigations, which is not only for explaining the ‘unexpected’ experimental observations, but also for accelerating the search of the anticipated room-temperature superconductivity in this class of novel materials.

Acknowledgements H.W. is thankful to G.T. Liu, H.B. Wang and M. Shiga for valuable discussions, and to L. Ma and X.L. Huang for the experimental EoS and XRD data. The project is supported by the National Natural Science Foundation of China (Grant No. 11974135 and 11974134), the Team program of the Natural Science Foundation of Heilongjiang Province, China (No. TD2021E005), and the Natural Sciences and Engineering Research Council of Canada. We used the computing facilities provided by ChinaHPC Cloud Computing Center.

Figure Captions

Figure 1. The volume shifts induced by nuclear thermal motions (δV_T) and nuclear quantum motions (δV_Q), and the sum of them (δV) in CaH₆ (a) and CaH_{5.5} (b).

Figure 2. (a) The quantum EoSs simulated at 300 K for CaH_{5.5}, CaH_{5.74} and CaH₆ hydrides compared to experimental data measured at room temperatures by Ma *et. al.*[25]. The insert structure above the EoSs is CaH₆, with Ca and H atom presented by big and small balls, respectively. (b) The quantum $N(\epsilon_F)$ of CaH_{6- δ} at 300 K and temperatures closing to experimental T_c , with distributions and standard errors shown in Fig. S3. The $N(\epsilon_F)$ of CaH_{6- δ} with δ of 0-0.33, CaH_{5.5} and CaH₆ derived from rigid band model (RBM) of the electronic structure of static CaH₆ were also shown for comparison.

Figure 3. (a) The $\langle u^2 \rangle$ of quantum and classical CaH_{5.74} at pressure of 160 GPa and various temperatures, compared to that of quantum CaH₆ at the same pressure and 300 K. (b) The $g(r)$ of quantum CaH_{5.74} at 160 GPa and various temperatures compared to that of quantum LaH_{9.63} at 163 GPa and 240 K. (c) The $f(\omega)$ of calcium and hydrogen in quantum CaH_{5.74} at 160 GPa and various temperatures.

Figure 1

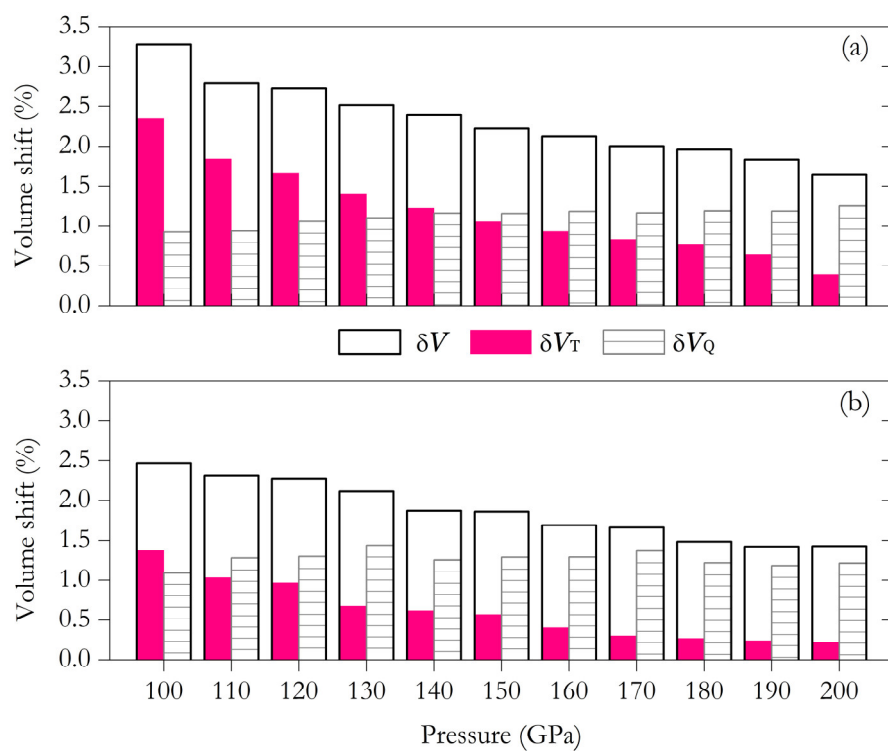


Figure 1. The volume shifts induced by nuclear thermal motions (δV_T) and nuclear quantum motions (δV_Q), and the sum of them (δV) in CaH_6 (a) and $\text{CaH}_{5.5}$ (b).

Figure 2

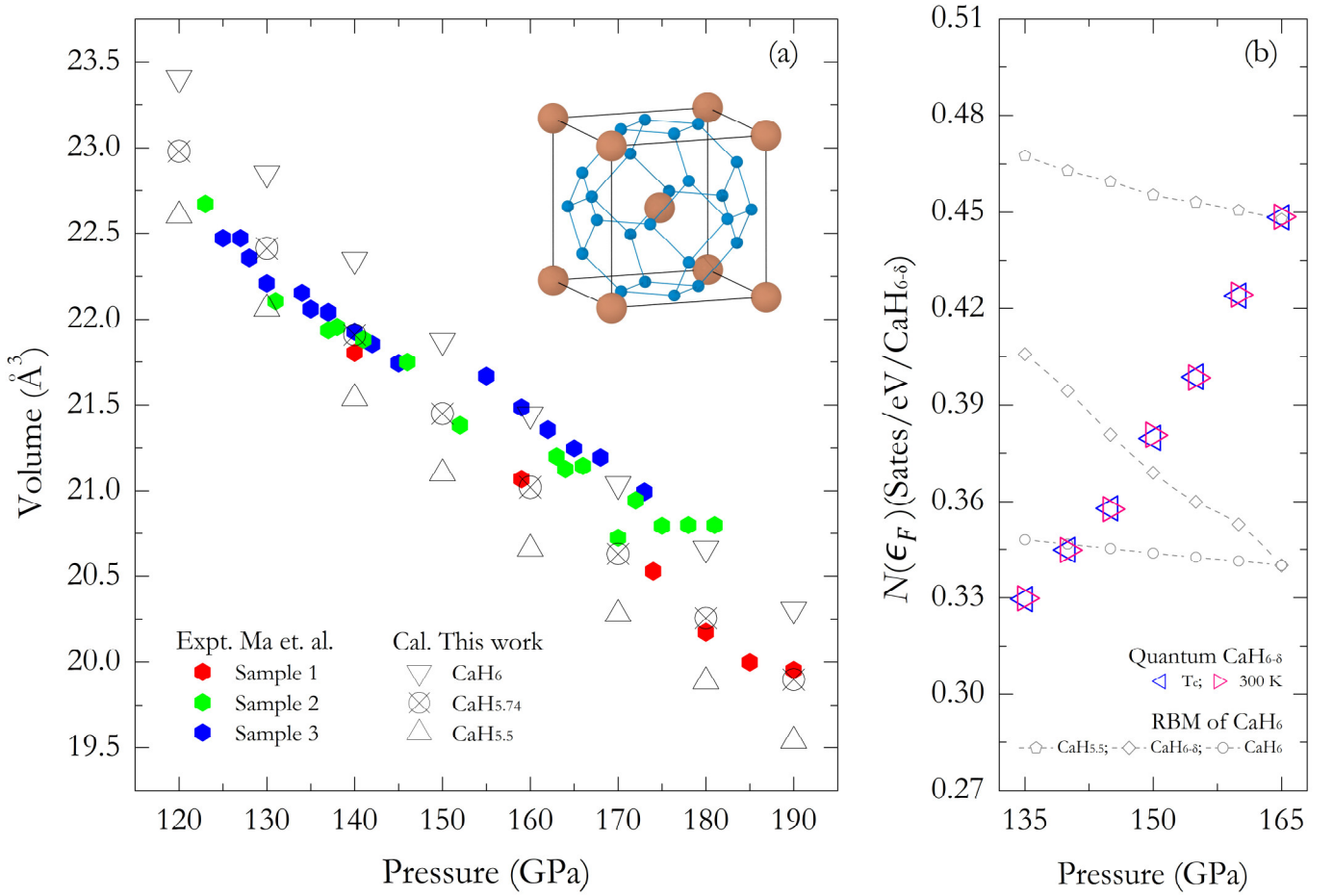


Figure 2. (a) The quantum EoSs simulated at 300 K for $\text{CaH}_{5.5}$, $\text{CaH}_{5.74}$ and CaH_6 hydrides compared to experimental data measured at room temperatures by Ma *et. al.*[25]. The insert structure above the EoSs is CaH_6 , with Ca and H atom presented by big and small balls, respectively. (b) The quantum $N(\epsilon_F)$ of $\text{CaH}_{6-\delta}$ at 300 K and temperatures closing to experimental T_c , with distributions and standard errors shown in Fig. S3. The $N(\epsilon_F)$ of $\text{CaH}_{6-\delta}$ with δ of 0-0.33, $\text{CaH}_{5.5}$ and CaH_6 derived from rigid band model (RBM) of the electronic structure of static CaH_6 were also shown for comparison.

Figure 3

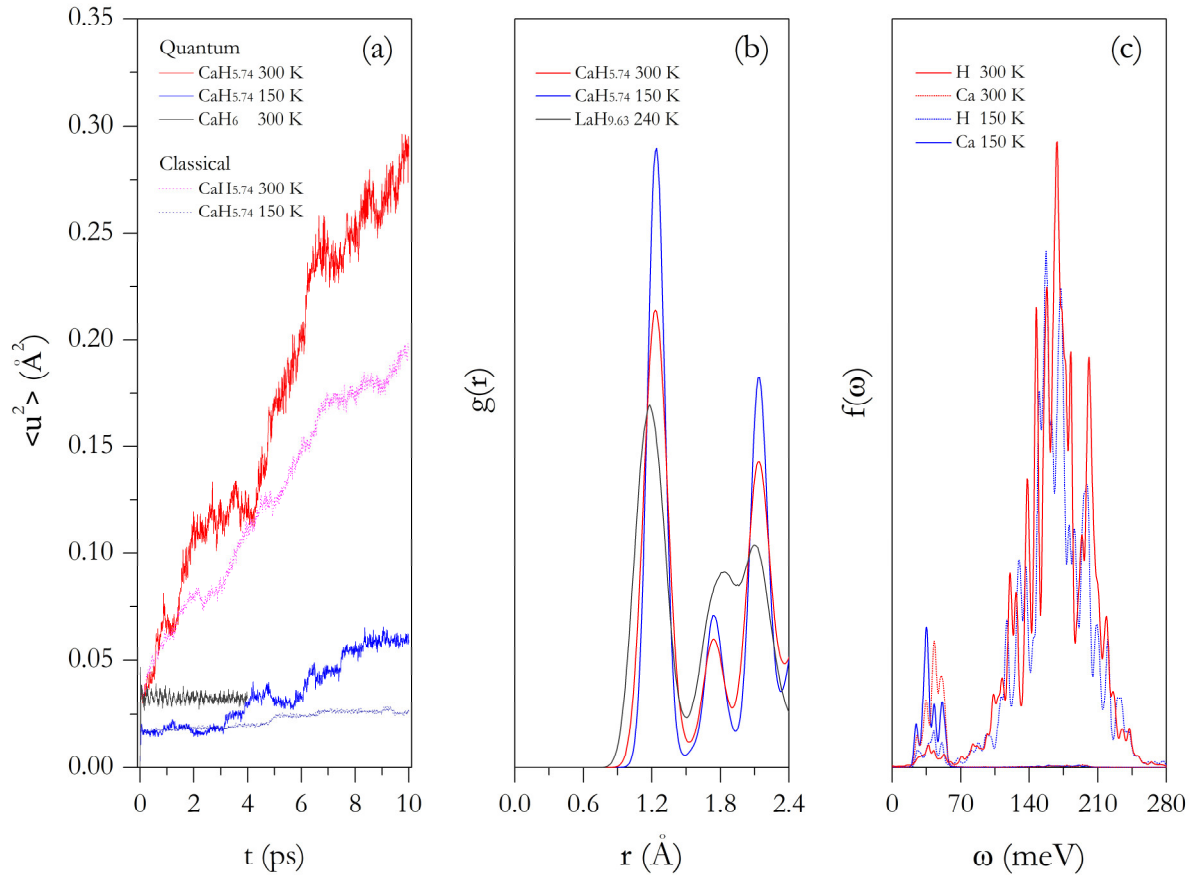


Figure 3. (a) The $\langle u^2 \rangle$ of quantum and classical $\text{CaH}_{5.74}$ at pressure of 160 GPa and various temperatures, compared to that of quantum CaH_6 at the same pressure and 300 K. (b) The $g(r)$ of quantum $\text{CaH}_{5.74}$ at 160 GPa and various temperatures compared to that of quantum $\text{LaH}_{9.63}$ at 163 GPa and 240 K. (c) The $f(\omega)$ of calcium and hydrogen in quantum $\text{CaH}_{5.74}$ at 160 GPa and various temperatures.

References

- [1] N. W. Ashcroft, *Phys. Rev. Lett.* **21**, 1748 (1968).
- [2] E. Wigner and H. B. Huntington, *J. Chem. Phys.* **3**, 764 (1935).
- [3] P. Loubeyre, F. Occelli, and P. Dumas, *Nature* **577**, 631 (2020).
- [4] E. Gregoryanz, C. Ji, P. Dalladay-Simpson, B. Li, R. T. Howie, and H. K. Mao, *Matter Radiat. Extremes* **5**, 038101 (2020).
- [5] M. I. Eremets, V. S. Minkov, P. P. Kong, A. P. Drozdov, S. Chariton, and V. B. Prakapenka, *Nat. Commun.* **14**, 907 (2023).
- [6] X. Zhong, J. S. Tse, R. J. Hemley, and H. Liu, *Innovation* **3**, 100226 (2022).
- [7] L. Monacelli, M. Casula, K. Nakano, S. Sorella, and F. Mauri, *Nat. Phys.* **19**, 845 (2023).
- [8] H. Wang, J. S. Tse, K. Tanaka, T. Iitaka, and Y. Ma, *Proc. Natl. Acad. Sci. U.S.A.* **109**, 6463 (2012).
- [9] M. Somayazulu, M. Ahart, A. K. Mishra, Z. M. Geballe, M. Baldini, Y. Meng, V. V. Struzhkin, and R. J. Hemley, *Phys. Rev. Lett.* **122**, 027001 (2019).
- [10] A. P. Drozdov *et al.*, *Nature* **569**, 528 (2019).
- [11] P. Kong *et al.*, *Nat. Commun.* **12**, 5075 (2021).
- [12] I. A. Troyan *et al.*, *Adv. Mater.* **33**, 2006832 (2021).
- [13] D. V. Semenok *et al.*, *Mater. Today* **48**, 18 (2021).
- [14] J. A. Flores-Livas, L. Boeri, A. Sanna, G. Profeta, R. Arita, and M. Eremets, *Phys. Rep.* **856**, 1 (2020).
- [15] C. J. Pickard, I. Errea, and M. I. Eremets, *Ann. Rev. Condens. Matt. Phys.* **11**, 57 (2020).
- [16] B. Lilia *et al.*, *J. Phys.: Condens. Matter* **34**, 183002 (2022).
- [17] C. S. Zha, Z. Liu, M. Ahart, R. Boehler, and R. J. Hemley, *Phys. Rev. Lett.* **110**, 217402 (2013).
- [18] N. D. Drummond, B. Monserrat, J. H. Lloyd-Williams, P. L. Ríos, C. J. Pickard, and R. J. Needs, *Nat. Commun.* **6**, 7794 (2015).
- [19] H. Liu and Y. Ma, *Phys. Rev. Lett.* **110**, 025903 (2013).
- [20] A. F. Goncharov, I. Chuvashova, C. Ji, and H. K. Mao, *Proc. Natl. Acad. Sci. U.S.A.* **116**, 25512 (2019).
- [21] I. Errea *et al.*, *Nature* **578**, 66 (2020).
- [22] H. Wang, P. T. Salzbrenner, I. Errea, F. Peng, Z. Lu, H. Liu, L. Zhu, C. J. Pickard, and Y. Yao, *Nat. Commun.* **14**, 1674 (2023).
- [23] X. Li *et al.*, *Nat. Commun.* **10**, 3461 (2019).
- [24] D. V. Semenok *et al.*, *Mater. Today* **33**, 36 (2020).
- [25] L. Ma *et al.*, *Phys. Rev. Lett.* **128**, 167001 (2022).
- [26] Z. Li *et al.*, *Nat. Commun.* **13**, 2863 (2022).
- [27] L. Ma *et al.*, *Phys. Rev. Res.* **3**, 043107 (2021).
- [28] A. R. H. R. P. Feynman, and D. F. Styer, *Quantum Mechanics and Path Integrals* (Courier Corporation, New York, 2010).
- [29] M. Shiga, M. Tachikawa, and S. Miura, *J. Chem. Phys.* **115**, 9149 (2001).
- [30] F. Birch, *Phys. Rev.* **71**, 809 (1947).
- [31] P. Vajda, in *Handbook on the Physics and Chemistry of Rare Earths* (Elsevier, 1995), pp. 207.
- [32] I. G. Ratishvili, P. Vajda, A. Boukraa, and N. Z. Namoradze, *Phys. Rev. B* **49**, 15461 (1994).
- [33] W. Chen, D. V. Semenok, X. Huang, H. Shu, X. Li, D. Duan, T. Cui, and A. R. Oganov, *Phys. Rev. Lett.* **127**, 117001 (2021).
- [34] See Supplemental Material at <http://link.aps.org/supplemental/xx.xxxx/PhysRevLett.xxx.xxxx> for supplemental figures and computational details, which includes Refs. [35-38].
- [35] G. Kresse and J. Furthmüller, *Phys. Rev. B* **54**, 11169 (1996).
- [36] J. P. Perdew, K. Burke, and M. Ernzerhof, *Phys. Rev. Lett.* **77**, 3865 (1996).
- [37] P. E. Blöchl, O. Jepsen, and O. K. Andersen, *Phys. Rev. B* **49**, 16223 (1994).
- [38] P. E. Blöchl, *Phys. Rev. B* **50**, 17953 (1994).
- [39] L. Boeri, in *Handbook of Materials Modeling: Applications: Current and Emerging Materials*, edited by W. Andreoni, and S. Yip (Springer International Publishing, Cham, 2020), pp. 73.
- [40] J. Bardeen, L. N. Cooper, and J. R. Schrieffer, *Phys. Rev.* **108**, 1175 (1957).
- [41] H. Wang, Y. Yao, F. Peng, H. Liu, and R. J. Hemley, *Phys. Rev. Lett.* **126**, 117002 (2021).
- [42] I. Errea, *J. Phys.: Condens. Matter* **34**, 231501 (2022).